Appl. Math. Mech. -Engl. Ed., **38**(11), 1601–1612 (2017)
DOI 10.1007/s10483-017-2279-9

Applied Mathematics and Mechanics (English Edition)

Interaction of weak free-stream disturbance with an oblique shock: validation of the shock-capturing method*

Caihong SU†, Jinlei GENG

Department of Mechanics, Tianjin University, Tianjin 300072, China

Abstract Transition prediction is of great importance for the design of long distance flying vehicles. It starts from the problem of receptivity, i.e., how external disturbances trigger instability waves in the boundary layer. For super/hypersonic boundary layers, the external disturbances first interact with the shock ahead of the flying vehicles before entering the boundary layer. Since direct numerical simulation (DNS) is the only available tool for its comprehensive and detailed investigation, an important problem arises whether the numerical scheme, especially the shock-capturing method, can faithfully reproduce the interaction of the external disturbances with the shock, which is so far unknown. This paper is aimed to provide the answer. The interaction of weak disturbances with an oblique shock is investigated, which has a known theoretical solution. Numerical simulation using the shock-capturing method is conducted, and results are compared with those given by theoretical analysis, which shows that the adopted numerical method can faithfully reproduce the interaction of weak external disturbances with the shock.

Key words shock, high speed flow, free-stream disturbance, shock-capturing

Chinese Library Classification O354
2010 Mathematics Subject Classification 76J20, 76K05

Nomenclature

Ma,	Mach number;
$\boldsymbol{u}$,	velocity normal to the shock;
$\boldsymbol{v}$,	velocity tangential to the shock;
ρ,	density;
p,	pressure;
ω,	frequency;
$\boldsymbol{k}$,	wave vector with components (k_x, k_y);
λ_x, λ_y,	wave lengths in x- and y-axes;
θ_1,	angle of incidence of wave relative to x-axis;
θ_2,	angle of divergence of acoustic wave relative to x-axis;
θ_3,	angle of divergence of entropy/vortical wave relative to x-axis;
β,	angle between flow velocity and shock;
c,	sound speed;
$\boldsymbol{v}_{\mathrm{g}}$,	group velocity;
γ,	ratio of the specific heat capacities;
$\overline{(\cdot)}$,	unperturbed flow quantities;
$\delta(\cdot)$,	flow fluctuations;
$(\cdot)_{1,2}$,	quantities at upstream and downstream of the shock.

* Received Apr. 20, 2017 / Revised May 8, 2017
Project supported by the National Natural Science Foundation of China (Nos. 11472188 and 11332007) and the National Key Research and Development Program of China (No. 2016YFA0401200)
† Corresponding author, E-mail: su_ch@tju.edu.cn

1 Introduction

The prediction of laminar-turbulent transition is of great importance for the design of long distance flying vehicles[1], and it has been and still remains a subject of extensive investigation[2–4].

In designing flying vehicles, usually, experiment plays a very important role. Therefore, people expect that experiment can also be very helpful in the prediction of laminar-turbulent transition. For this purpose, quiet wind tunnels were designed and are being used. Generally speaking, to simulate the real flight, certain similarity rules have to be satisfied, as shown in Ref. [5]. However, to simulate the laminar-turbulent transition of the boundary layer of the super/hypersonic flying vehicles, more stringent requirements are necessary. For example, first, transition location is sensitive to viscosity, which depends on temperature. Thus, the temperature distribution of the flow fields must be the same for both the real flying vehicle and the model. Second, transition location is also sensitive to the free-stream disturbances. Thus, the disturbances in the free stream in their non-dimensional form must be the same for both the experiment and the real flying vehicle. Obviously, these two requirements are impossible to be realized in practice.

The other way to model the transition process is to do direct numerical simulation (DNS), if computer resource allows. In this case, proper numerical scheme has to be used. One criterion for its choice is how well it can treat the interaction of the disturbances with the shock, because, for super/hypersonic flight, disturbances in the oncoming flow would certainly first interact with the shock, and then disturbances behind the shock resulting from the interaction would interact with the boundary layer to trigger instability waves in the boundary layer. Therefore, whether the numerical scheme can faithfully reproduce the interaction is crucial for its success. Usually, the shock-fitting method can produce reliable results[6–10], but it can hardly be used for three-dimensional problems[11]. There have been people using the shock-capturing scheme for this purpose[12–14]. However, they assumed implicitly that the shock-capturing scheme can faithfully reproduce the disturbances behind the shock, but with no proof or convincing discussion to confirm its reliability. Therefore, how well the shock-capturing scheme can reproduce the interaction of small amplitude disturbances with the shock is a problem worth being investigated, as pointed out in the latest review article "Two problems in the transition and turbulence for the near space hypersonic flying vehicles" by Zhou and Zhang[15].

Therefore, in this paper, our main concern is the accuracy of shock-capturing method in its application to the interaction of small disturbance and the shock.

In a linear regime, a general small amplitude free-stream disturbance in a uniform flow can be decomposed of three elementary types of components[16], namely, acoustic wave, vorticity wave, and entropy wave. The acoustic wave propagates at the speed of sound relative to the moving fluids, while the vorticity and entropy waves are convected passively by the mean flow. Furthermore, the acoustic wave can also be distinguished as fast or slow acoustic wave according to whether its group velocity is larger or smaller than the moving velocity of the flow. All types of disturbances may be generated behind the shock no matter what type of disturbance wave interacts with the shock[17].

However, in the high altitude atmosphere, the velocity and temperature are bound to be non-uniform, which are the cause of entropy wave and vorticity wave, but there can hardly be external object generating acoustic waves, while the generation of sound wave by the motion of the fluid itself, is far less effective. Therefore, in this paper, we only pay attention to the incidence of entropy and vorticity waves. Besides, for super/hypersonic flying vehicles, the free stream disturbances can always be regarded as small amplitude disturbances.

Thus, the problem we are dealing with is, when small amplitude free-stream disturbances meet a stationary oblique shock, what kind of disturbances would be induced downstream of the

shock, and whether the numerical simulation using the shock-capturing scheme can obtain the results with sufficient accuracy. For this purpose, we need reliable theoretical or experimental results to compare with numerical results. Reference [17] can serve for this purpose. The paper is organized as follows. In Section 2, we use the method of McKenzie and Westphal[17] and the errata given by Anyiwo and Bushnell[18] to analyze the interaction of small amplitude disturbances with an oblique shock. In Section 3, we perform numerical simulations using the shock-capturing scheme with moderate order of accuracy for the same problem. In Section 4, numerical results are compared with the theoretical results to check if the shock-capturing method can produce sufficiently accurate results. In Section 5, we conclude the paper with a summary discussion.

2 Theoretical analysis

The method of McKenzie and Westphal[17] is adopted to formulate the problem. For the readers' convenience, we outline the main procedures. In addition to their work, in Subsection 2.2, we complement another physical condition to remove the nonphysical solution that may arise for the solutions of wave vectors. Furthermore, we deduce the condition to determine whether fast or slow acoustic wave can be generated behind the shock, which is also in Subsection 2.2.

2.1 Problem formulation

The coordinate system (x, y) is set up, as shown in Fig. 1, where x and y are normal to and along with the shock, respectively. $\boldsymbol{u}_1$ and $\boldsymbol{u}_2$ denote the velocities of the uniform flows at upstream and downstream of the shock, respectively. Their angles with respect to the shock are denoted by β_1 and β_2, respectively. We assume that the free-stream disturbance, which can be an acoustic, entropy, or vorticity wave, is of the form $\delta A \mathrm{e}^{\mathrm{i}(k_x x + k_y y - \omega t)}$, where k_x and k_y are the components of wave vector $\boldsymbol{k}$ in (x, y), ω is the frequency, and δA represents the amplitude of any perturbed quantity. $\boldsymbol{k}_1$, $\boldsymbol{k}_2$, and $\boldsymbol{k}_3$ represent the wave vectors of the incident wave, the acoustic wave leaving the shock, and the diverging entropy-vorticity wave, respectively. Their angles of wave vector with respect to the x-axis are θ_1, θ_2, and θ_3, respectively.

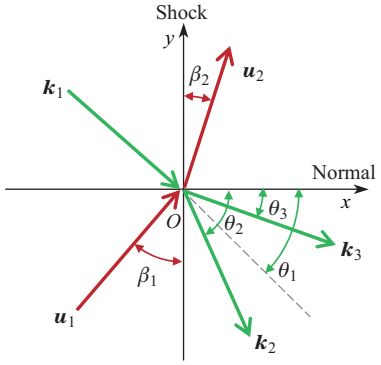

Fig. 1 Schematic diagram of the disturbances and the shock

The total flow field can be written as the summation of steady base flow and a small perturbed quantity as follows:

$$(\rho, u, v, p) = (\overline{\rho}, \overline{u}, \overline{v}, \overline{p}) + (\delta\rho, \delta u, \delta v, \delta p)\mathrm{e}^{\mathrm{i}(k_x x + k_y y - \omega t)}. \tag{1}$$

Substitute (1) into the linearized Euler equations and solve the eigenvalue systems. We can get the dispersion relations and the corresponding eigenvectors for three elementary types of free-stream disturbances.

For acoustic waves, the dispersion relation is

$$\omega - \overline{u}k_x - \overline{v}k_y = \pm c|\boldsymbol{k}|, \tag{2}$$

and the corresponding eigenvector is

$$(\delta\rho, \delta u, \delta v, \delta p) = \left(1, \pm\frac{c\cos\theta}{\overline{\rho}}, \pm\frac{c\sin\theta}{\overline{\rho}}, c^2\right), \tag{3}$$

where c is the sound speed, $|\boldsymbol{k}| = \sqrt{k_x^2 + k_y^2}$, and θ is the angle between the wave vector and the x-axis. Plus (minus) sign corresponds to fast (slow) acoustic waves.

For entropy and vorticity waves, the dispersion relations are both

$$\omega - \overline{u}k_x - \overline{v}k_y = 0, \tag{4}$$

and the eigenvectors are, respectively,

$$(\delta\rho, \delta u, \delta v, \delta p) = (1, 0, 0, 0), \tag{5}$$

$$(\delta\rho, \delta u, \delta v, \delta p) = (0, -\sin\theta, \cos\theta, 0). \tag{6}$$

It is worth noting that the direction of $\boldsymbol{k}$ indicates the phase direction of the disturbance, which is perpendicular to the wavefronts. It is different from the direction of group velocity $\boldsymbol{v}_{\rm g}$, i.e., ray. We depict the phase and the ray for the incident entropy/vorticity wave in Fig. 2. For the entropy/vorticity wave, $\boldsymbol{v}_{\rm g}$ is the velocity of the moving fluid, i.e., $\boldsymbol{u}_1$, while for the acoustic wave, the group velocity is given by

$$\boldsymbol{v}_{\rm g} = \frac{\partial\omega}{\partial\boldsymbol{k}} = \boldsymbol{u} \pm c\frac{\boldsymbol{k}}{|\boldsymbol{k}|}, \tag{7}$$

where plus (minus) corresponds to fast (slow) acoustic wave.

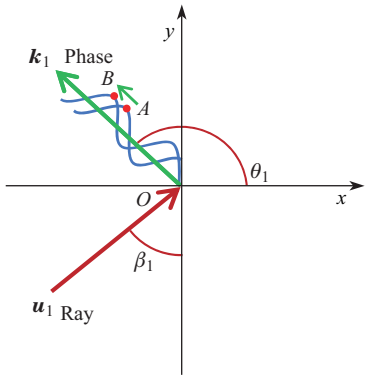

Fig. 2 Schematic diagram of the phase and ray for the entropy/vortical wave

2.2 Wave vectors

Three conditions need to be satisfied across the shock:

(i) The frequency is continuous on both sides of the shock.

(ii) The component of wave vector tangential to the shock, say, k_y is continuous.

(iii) The component of group velocity normal to the shock should be larger than zero.

Condition (iii) is deduced from the assumption that all the disturbances behind the shock should propagate downstream, which is true for the interaction taking place in the free space.

Since the waves are of small amplitude, these conditions can be applied to the unperturbed shock in the linear approximation. For acoustic waves generated by the entropy/vorticity wave, considering the dispersion relations given by (2) and (4), the application of Condition (i) gives

$$\overline{u}_1 k_{1x} + \overline{v}_1 k_{1y} = \overline{u}_2 k_{2x} + \overline{v}_2 k_{2y} \pm c_2|\boldsymbol{k}_2|, \tag{8}$$

where $|\boldsymbol{k}_2| = \sqrt{k_{2x}^2 + k_{2y}^2}$, and subscripts 1 and 2 of the unperturbed quantities denote the quantities at upstream and downstream of the shock, respectively. From the first-order of continuity of unperturbed velocity tangential to the shock, we have $\overline{v}_1 = \overline{v}_2$. From Condition (ii), we have $k_{1y} = k_{2y} = k_y$, and then (8) reduces to

$$\overline{u}_1 k_{1x} = \overline{u}_2 k_{2x} \pm c_2 \sqrt{k_{2x}^2 + k_y^2}, \tag{9}$$

where $\overline{u}_2$ and c_2 can be computed by the Rankine-Hugoniot (R-H) conditions across the unperturbed shock. k_{2x} can be solved from (9), and then the angle of the wave vector is given by $\tan\theta_2 = k_y/k_{2x}$.

Similarly, for the entropy/vorticity wave behind the shock, the wave vector can be solved by

$$\overline{u}_1 k_{1x} = \overline{u}_2 k_{3x}.$$

According to the existent condition of (9), we can deduce that the incident angle θ_1 should satisfy (details are referred to Appendix A)

$$\tan^2\theta_1 \leqslant \frac{Ma_{1\mathrm{n}}^2}{(1 - Ma_{2\mathrm{n}}^2)R^2}, \quad R = \frac{c_2}{c_1}, \tag{10}$$

where the subscript n represents components normal to the shock. Considering that the physical frequency should be larger than zero, by rewriting the dispersion relation of (4), the incident angle θ_1 for the entropy/vorticity wave should also satisfy

$$\cos\left(\frac{\pi}{2} - \beta_1 - \theta_1\right) = \frac{\omega}{|\boldsymbol{u}_1||\boldsymbol{k}_1|} > 0,$$

and thus

$$-\beta_1 < \theta_1 < \pi - \beta_1. \tag{11}$$

Combining (10) and (11), we depict the range of incident angle for entropy/vorticity wave to generate acoustic wave in Fig. 3. In Region Ⅰ, only fast acoustic wave can be generated behind the shock. In Region Ⅱ, only a slow acoustic wave can be generated. Outside Regions Ⅰ and Ⅱ, no acoustic wave can be generated.

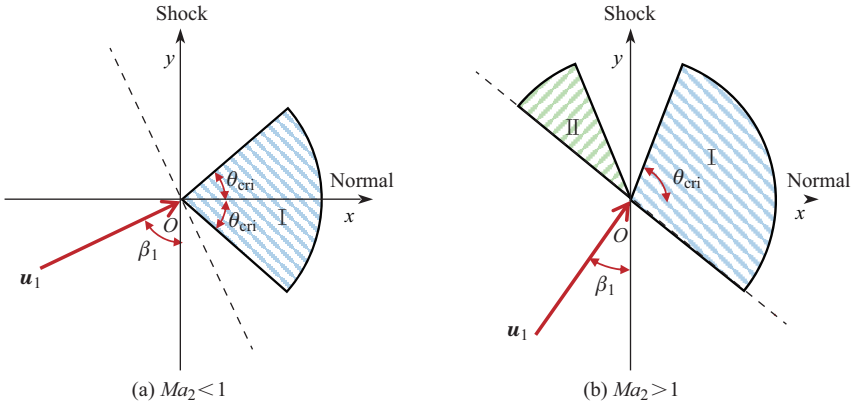

Fig. 3 Range of incident angle to generate acoustic waves

For $Ma_2 < 1$,

$$\text{Region I:} \ -\theta_{\mathrm{cri}} \leqslant \theta_1 \leqslant \theta_{\mathrm{cri}}, \quad \theta_{\mathrm{cri}} = \arctan\frac{Ma_{1\mathrm{n}}}{\sqrt{(1 - Ma_{2\mathrm{n}}^2)R}}.$$

For $Ma_2 > 1$,

$$\text{Region I}: \quad -\beta_1 < \theta_1 \leqslant \theta_{\rm cri}.$$
$$\text{Region II}: \quad \pi - \theta_{\rm cri} < \theta_1 < \pi - \beta_1.$$

2.3 Wave amplitude

Small perturbations are introduced in the R-H jump conditions on either side of the shock, and the linearized jump relations for small perturbations across the shock obtained are

$$\overline{\rho}_1\delta u_{1\rm n} + \overline{u}_{1\rm n}\delta\rho_1 = \overline{\rho}_2\delta u_{2\rm n} + \overline{u}_{2\rm n}\delta\rho_2, \tag{12a}$$
$$\delta p_1 + 2\overline{\rho}_1\overline{u}_{1\rm n}\delta u_{1\rm n} + \overline{u}_{1\rm n}^2\delta\rho_1 = \delta p_2 + 2\overline{\rho}_2\overline{u}_{2\rm n}\delta u_{2\rm n} + \overline{u}_{2\rm n}^2\delta\rho_2, \tag{12b}$$
$$\delta\boldsymbol{u}_{1\rm T} = \delta\boldsymbol{u}_{2\rm T}, \tag{12c}$$
$$\delta h_1 + \overline{u}_{1\rm n}\delta u_{1\rm n} = \delta h_2 + \overline{u}_{2\rm n}\delta u_{2\rm n}, \tag{12d}$$

where subscripts n and T denote the components normal and tangential to the shock, respectively. h is enthalpy.

Assume that the state equation is in the form of $\rho = \rho(p, s)$, where s is entropy. Small fluctuations in density are related to pressure and entropy fluctuations by

$$\delta\rho = \Big(\frac{\partial\rho}{\partial p}\Big)_s\delta p + \Big(\frac{\partial\rho}{\partial s}\Big)_p\delta s = \frac{\delta p}{c^2} + r\delta s, \tag{13}$$

where $r = -\frac{\rho}{c_p}$ for a perfect gas, and c_p is the heat capacity at the constant pressure.

Combine the shock adiabatic, which is in the form of $\rho_2 = \rho_2(p_2, \rho_1, p_1)$, and the relation of small-perturbation of pressure, entropy, and density can be obtained to replace (12d),

$$\delta p_2(c_2^{-2} - Q) + r_2\delta s_2 = P\delta p_1 + Wr_1\delta s_1, \tag{14}$$

where

$$Q = \frac{1}{c_2^2 Ma_{1\rm n}^2 Ma_{2\rm n}^2}, \quad P = \frac{\gamma-1}{\gamma+1}\frac{(Ma_{1\rm n}^2-1)^2}{c_2^2 Ma_{1\rm n}^2 Ma_{2\rm n}^2}, \quad W = \frac{\overline{\rho}_2}{\overline{\rho}_1}.$$

The deformation of the shock can be assumed to be in the same form of the incident disturbance,

$$x = f(y,t) = \eta\exp(\mathrm{i}(k_y y - \omega t)), \tag{15}$$

where η is the amplitude of the shock distortion and obviously $\eta \ll 1$. The velocity of the shock $\boldsymbol{u}_{\rm s}$ is

$$\boldsymbol{u}_{\rm s} = \Big(\frac{\partial f}{\partial t} + \frac{\partial f}{\partial y}\frac{\partial y}{\partial t}, \frac{\partial y}{\partial t}\Big). \tag{16}$$

Let $\delta d = \frac{\partial f}{\partial t}$, and thus $\frac{\partial f}{\partial y} = \frac{k_y\delta d}{\omega}$. The velocity of the fluid relative to the shock is $\boldsymbol{u}+\delta\boldsymbol{u}-\boldsymbol{u}_{\rm s}$. Substitute its normal and tangential components into (12a)–(12c), and the term $\frac{\partial y}{\partial t}$ can be eliminated. Combining with (13) and (14), a system of four linear equations with four unknowns, i.e., δd, δp_2, δs_2, and δu_2, is obtained, which can be solved.

3 Numerical simulation

Numerical simulation is performed to get the same result for the interaction of the small disturbance with the shock. The governing equations are the two-dimensional unsteady compressible Euler equations in the conservation form,

$$\frac{\partial U}{\partial t} + \frac{\partial E}{\partial x} + \frac{\partial F}{\partial y} = 0, \tag{17}$$

where U is the flow quantities, and E and F are the nonlinear terms, including the pressure gradient. The Cartesian coordinate (x, y) is set as shown in Fig. 1. The unperturbed flow quantities before the shock, i.e., $\overline{u}_1$, $\overline{\rho}_1$, and $\overline{\rho}_1\overline{u}_1^2$, are used to non-dimensionalize the velocity, density, and pressure, respectively. We choose a common and moderate accuracy shock-capturing scheme, i.e., a third-order weighted essentially nonoscillatory (WENO) scheme, to test its accuracy to simulate the fluctuations behind the shock. A third-order total-variation-diminishing (TVD) Runge-Kutta scheme is used for time advancement. As for the boundary conditions, the periodic condition is used for the upper and lower boundaries, and a sponge region is used as outflow boundary condition.

For our problem, since the wave number keeps unchanging in the y-direction, the computation can actually be reduced to a one-dimensional problem by performing the Fourier transform in y. However, in this paper, we still perform a two-dimensional computation with only considering one wave length in the y-direction so that the total computational work is well acceptable. Figure 4 shows the distribution of the unperturbed shock which locates at $x = 0.3$. The Mach number of the oncoming flow is taken as 8, and the angle between the flow and the shock β_1 is 35°.

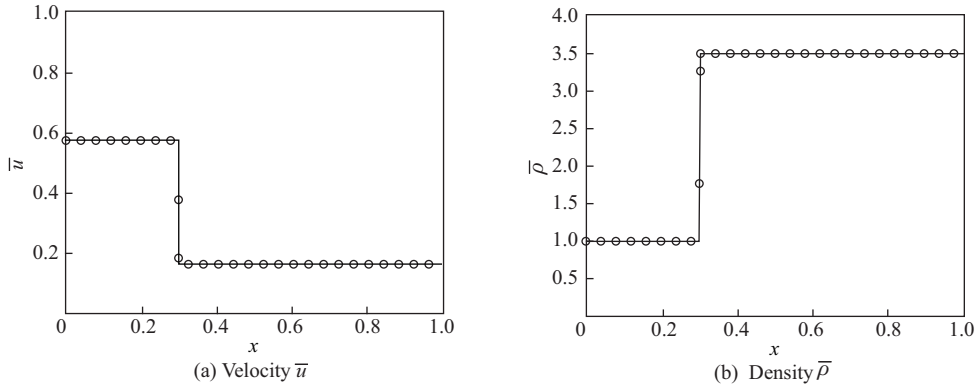

Fig. 4 The unperturbed shock

4 Results and discussion

The computation is performed first without imposing any disturbance. When the flow filed is completely steady, the small amplitude disturbance is introduced at the inlet. The flow quantities at the inlet are given by

$$\text{entropy wave: } \begin{pmatrix} \rho \\ u \\ v \\ p \end{pmatrix} = \begin{pmatrix} \overline{\rho} \\ \overline{u} \\ \overline{v} \\ \overline{p} \end{pmatrix} + \begin{pmatrix} \delta A \\ 0 \\ 0 \\ 0 \end{pmatrix} \mathrm{e}^{\mathrm{i}(k_y y - \omega t)}, \tag{18}$$

$$\text{vorticity wave: } \begin{pmatrix} \rho \\ u \\ v \\ p \end{pmatrix} = \begin{pmatrix} \overline{\rho} \\ \overline{u} \\ \overline{v} \\ \overline{p} \end{pmatrix} + \begin{pmatrix} 0 \\ -\delta A \sin\theta_1 \\ \delta A \cos\theta_1 \\ 0 \end{pmatrix} \mathrm{e}^{\mathrm{i}(k_y y - \omega t)}, \tag{19}$$

where $\delta A = 10^{-5}$, $k_y = 16\pi$, $\theta_1 = 45°$, and ω can be computed from the dispersion relation, i.e., $\omega = (\overline{u}_1/\tan\theta_1 + \overline{v}_1)k_y = 66.4$. Note that there is no length scale in our problem. Therefore, the value of k_y is taken arbitrarily. The flow parameters and quantities are given in Table 1. Case 1 and Case 2 correspond to the cases where the flow behind the shock is subsonic and supersonic, respectively.

Table 1 The flow parameters ($\gamma = 5/3$)

Case	β_1	Ma_1	$\overline{u}_1$	$\overline{v}_1$	β_2	Ma_2	$\overline{u}_2$
Case 1	65.89°	8.00	0.913	0.408	30.54°	0.906	0.241
Case 2	35.09°	8.00	0.575	0.818	11.34°	2.442	0.164

4.1 Case 1 where $Ma_2 < 1$

Figures 5(a)–5(c) show the instantaneous perturbations along x at a specific y location. At this time, the generated fast acoustic wave has already passed through the outlet boundary of the computational domain, while the entropy and vorticity waves still remain in the computational domain. As shown in Figs. 5(a) and 5(b), the density and streamwise velocity fluctuations show a pattern of a wave packet in the range of $x = 0.30$–0.70, where the transmitted entropy wave, the generated vorticity wave, and the fast acoustic wave are mixed. The pressure perturbation shown in Fig. 5(c) has a sine-wave pattern because only the generated acoustic wave has the component of pressure fluctuation.

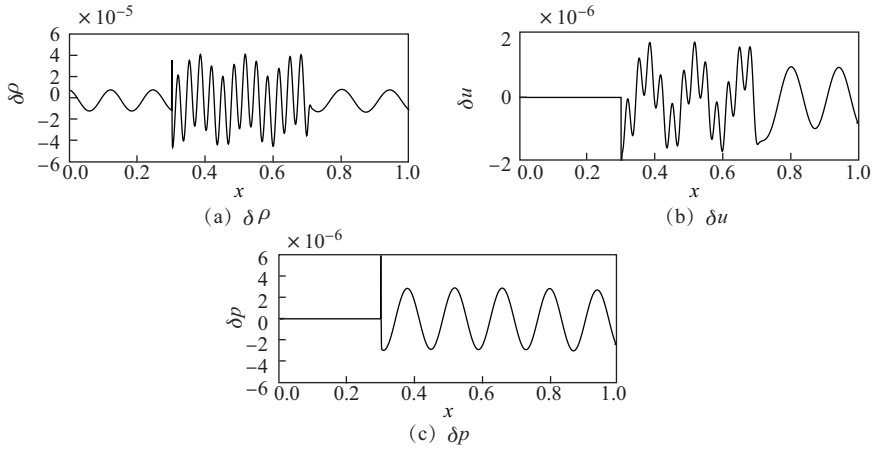

Fig. 5 Flow fluctuations for the incidence of entropy wave

Since there is no nonlinear interaction between disturbances, we can separate the different types of disturbance from the flow perturbation field. Figures 6(a) and 6(b) show $\delta\rho$ for the entropy wave and δu for the vorticity wave, respectively.

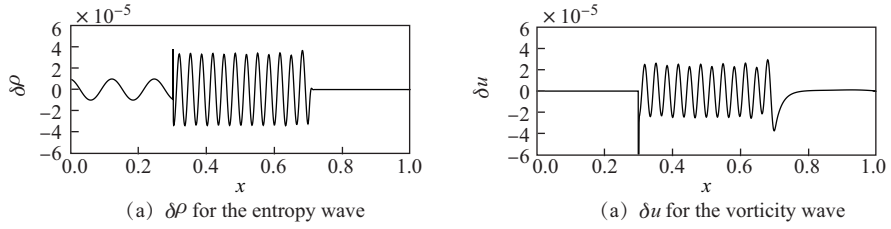

Fig. 6 Flow fluctuations of different types of disturbances

From the numerical results above, we can get the wave length of generated/transmitted wave along the x- and y-axes, respectively, i.e., λ_x, and λ_y. Then, the wave angle θ can be computed from

$$\tan\theta = \frac{\lambda_x}{\lambda_y}. \tag{20}$$

The wave length λ of transmitted/generated wave is given by

$$\lambda = \frac{\lambda_x \lambda_y}{\sqrt{\lambda_x^2 + \lambda_y^2}}. \tag{21}$$

Since we are especially interested in the acoustic wave generated behind the shock, to evaluate the efficiency of generation of the acoustic wave, a coefficient of generation is defined as, for the entropy incidence,

$$C = \frac{\delta p_2}{p_1 \delta A_{\mathrm{E}}/\rho_1},$$

and for the vortical incidence,

$$C = -\frac{\delta p_2}{p_1 \delta A_{\mathrm{V}}/|\boldsymbol{u}_1|},$$

where subscripts E and V denote the fluctuations of entropy and vorticity, respectively.

According to Section 2, the wave length of the disturbances behind the shock given by the theoretical analysis is

$$\text{acoustic wave: } \lambda_2 = (\overline{u}_2 \cos\theta_2 + \overline{v}_2 \sin\theta_2 \pm c_2)\frac{2\pi}{\omega}, \tag{22}$$

$$\text{entropy/vorticity wave: } \lambda_3 = (\overline{u}_2 \cos\theta_3 + \overline{v}_2 \sin\theta_3)\frac{2\pi}{\omega}, \tag{23}$$

where sign plus (minus) corresponds to fast (slow) acoustic wave.

We compare the numerical results with the theoretical results in Table 2. δp_{A} denotes the pressure fluctuation of acoustic wave. The negative value of δA_{V} means that its phase has a lag of π compared with the incident wave. We can see very good agreement between the results from the two methods. Furthermore, note that the pressure fluctuations, indicated as well as in the generation coefficient C, which represent the acoustic wave of more importance in the receptivity problem, are in perfect agreement.

Table 2 Comparison of results for the incidence of entropy wave

Method	θ_2	λ_2	θ_3	λ_3	δA_{E}	δA_{V}	δp_{A}	C
Numerical	48.47°	0.094	14.79°	0.032	3.3×10^{-5}	-2.1×10^{-6}	2.9×10^{-6}	0.29
Theoretical	48.59°	0.094	14.82°	0.032	2.8×10^{-5}	-2.3×10^{-6}	2.9×10^{-6}	0.29

We also use the vorticity wave as the inlet disturbance to perform the same computation. The comparison of results given by two methods is shown in Table 3. Also, very good agreement can be found.

Table 3 Comparison of results for the incidence of vorticity wave

Method	θ_2	λ_2	θ_3	λ_3	δA_{E}	δA_{V}	δp_{A}	C
Numerical	48.47°	0.094	14.79°	0.032	1.0×10^{-5}	1.2×10^{-5}	-4.5×10^{-6}	0.75
Theoretical	48.59°	0.094	14.82°	0.032	1.5×10^{-5}	1.2×10^{-5}	-4.5×10^{-6}	0.75

4.2 Case 2 where $Ma_2 > 1$

For the case that the flow is supersonic behind the shock, both slow and fast acoustic waves can be generated behind the shock. Two angles are chosen for the incident entropy wave, say, 45° and 135°. Table 4 shows the parameters used in two cases. Note that $\theta_1 = 45°$, which lies in Regions I of Fig. 3(b), while $\theta_1 = 135°$ lies in Region II. Therefore, Cases 2a and 2b correspond to the cases that fast and slow acoustic waves are generated behind the shock, respectively.

Table 4 Parameters of incident entropy wave

Case	θ_1	k_x	k_y	ω
Case 2a	45°	50.27	50.27	70.02
Case 2b	135°	−287.71	287.71	70.02

Figures 7(a)–7(d) show the instantaneous contour of flow fluctuations for Cases 2a and 2b at a specific time when the wave with higher group velocity has passed through the computational domain, while the other waves still remain in the domain. We compare the results with those given by theoretical analysis in Table 5. As before, very good agreement can be found. Especially, for the acoustic waves, the shock-capturing method gives very accurate results.

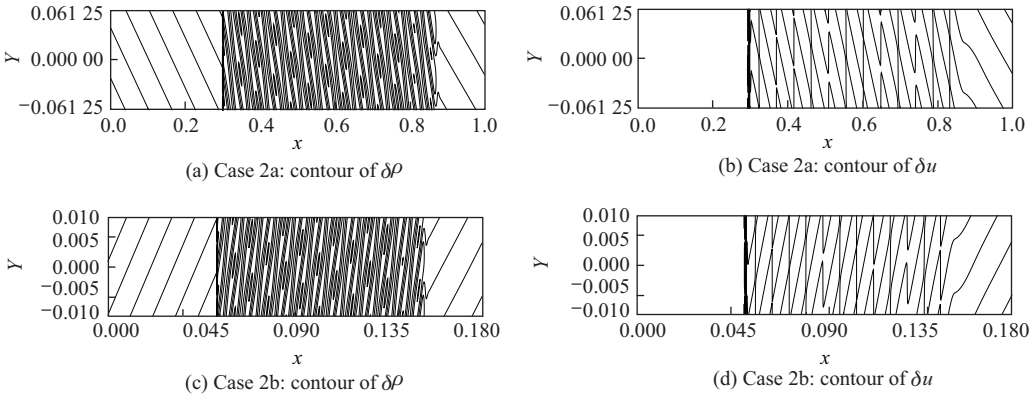

(a) Case 2a: contour of $\delta\rho$ (b) Case 2a: contour of δu

(c) Case 2b: contour of $\delta\rho$ (d) Case 2b: contour of δu

Fig. 7 Instantaneous contours of flow fluctuations

Table 5 Comparison between numerical and theoretical methods

Case	Method	θ_2	λ_2	θ_3	λ_3	$\delta A_{\rm E}$	$\delta A_{\rm V}$	$\delta p_{\rm A}$	C
Case 2a	Numerical	50.82°	0.097	15.94°	0.034	3.2×10^{-5}	-1.8×10^{-6}	1.1×10^{-6}	0.106
	Theoretical	50.80°	0.097	15.93°	0.034	2.8×10^{-5}	-1.6×10^{-6}	1.1×10^{-6}	0.106
Case 2b	Numerical	129.18°	0.017	164.07°	0.006	3.2×10^{-5}	1.8×10^{-6}	1.1×10^{-6}	0.106
	Theoretical	129.20°	0.017	164.07°	0.006	2.8×10^{-5}	1.6×10^{-6}	1.1×10^{-6}	0.106

It should be noticed that for Case 2b, the generated slow acoustic wave still propagates faster than the entropy/vorticity wave, whose group velocity is $\overline{u}_2$, so that it goes out of the computational domain first. This can be explained by recalling the group velocity of the acoustic wave in (7). For Case 2b, since $\cos\theta_2 < 0$, the x-component of group velocity is $v_{{\rm g}x} = \overline{u}_2 - c_2\cos\theta_2 > \overline{u}_2$. Therefore, we see that the slow acoustic wave goes out of the computational domain first.

Taking the vorticity wave as the inlet disturbance, no essential difference can be found. Therefore, we omit the results here.

5 Summary and conclusions

In this paper, the interaction of small amplitude free-stream disturbances with an oblique shock is investigated. Considering the real situation in high altitude environment that flying vehicles may encounter, only the incidence of entropy/vorticity wave is considered. The numerical simulation is performed, using a common and moderate order accuracy shock-capturing method, say, the third-order WENO. The results are compared with those given by theoretical

analysis. Satisfactory agreement is achieved, confirming that the shock-capturing method can faithfully reproduce the interaction of weak external disturbances with the shock.

Acknowledgements The first author would like to thank Professor Heng ZHOU in Tianjin University for his continuous encouragement and Professor Jisheng LUO in Tianjin University for his inspiring discussion and helpful suggestions.

References

[1] Reshotko, E. Transition issues for atmospheric entry. *Journal of Spacecraft and Rockets*, **45**(2), 161–164 (2008)

[2] Fedorov, A. V. Transition and stability of high-speed boundary layers. *Annual Review of Fluid Mechanics*, **43**, 79–95 (2011)

[3] Zhong, X. and Wang, X. Direct numerical simulation on the receptivity, instability and transition of hypersonic boundary layers. *Annual Review of Fluid Mechanics*, **44**, 527–561 (2012)

[4] Qin, F. and Wu, X. Response and receptivity of the hypersonic boundary layer past a wedge to free-stream acoustic, vortical and entropy disturbances. *Journal of Fluid Mechanics*, **797**, 874–915 (2016)

[5] Zhang, H. X. The similarity law for real gas flow (in Chinese). *Acta Aerodynamica Sinica*, **8**(1), 1–8 (1990)

[6] Zhong, X. Leading-edge receptivity to free-stream disturbance waves for hypersonic flow over a parabola. *Journal of Fluid Mechanics*, **441**, 315–367 (2001)

[7] Ma, Y. and Zhong, X. Receptivity of a supersonic boundary layer over a flat plate, part 1, wave structures and interactions. *Journal of Fluid Mechanics*, **488**, 31–78 (2003)

[8] Ma, Y. and Zhong, X. Receptivity of a supersonic boundary layer over a flat plate, part 2, receptivity to freestream sound. *Journal of Fluid Mechanics* **488**, 79–121 (2003)

[9] Ma, Y. and Zhong, X. Receptivity of a supersonic boundary layer over a flat plate, part 3, effects of different types of free-stream disturbances. *Journal of Fluid Mechanics*, **532**, 63–109 (2005)

[10] Ma, Y. and Zhong, X. Boundary-layer receptivity of Mach 7.99 flow over a blunt cone to free-stream acoustic waves. *Journal of Fluid Mechanics*, **556**(1), 55–103 (2006)

[11] Bonfiglioli, A., Grottadaurea, M., Paciorri, R., and Sabetta, F. An unstructured, three-dimensional, shock-fitting solver for hypersonic flows. *Computers and Fluids*, **73**, 162–174 (2013)

[12] Balakumar, P. Receptivity of a supersonic boundary layer to acoustic disturbances. *AIAA Journal*, **47**(5), 1069–1078 (2009)

[13] Balakumar, P. and Kegerise, M. A. Receptivity of hypersonic boundary layers over straight and flared cones. *AIAA Journal*, **53** (2010)

[14] Soudakov, V. G. Numerical simulation of hypersonic boundary layer receptivity to entropy and vorticity waves. *TsAGI Science Journal*, **44**(2), 205–217 (2013)

[15] Zhou, H. and Zhang, H. X. Two problems in the transition and turbulence for near space hypersonic flying vehicles (in Chinese). *Acta Aerodynamica Sinica*, **35**(2), 151–155 (2017)

[16] Kovasznay, L. S. G. Turbulence in supersonic flow. *Thermal Engineering*, **20**(10), 657–674 (1953)

[17] McKenzie, J. F. and Westphal, K. O. Interaction of linear waves with oblique shock waves. *Physics of Fluids*, **11**(11), 2350–2362 (1968)

[18] Anyiwo, J. C. and Bushnell, D. M. Turbulence amplification in shock-wave boundary-layer interaction. *AIAA Journal*, **20**(7), 893–899 (1982)

Appendix A

In this appendix, first, we prove that if $\theta_1 \in (-\frac{\pi}{2}, \frac{\pi}{2})$, no slow acoustic wave can be generated behind the shock, while if $\theta_1 \in (\frac{\pi}{2}, \frac{3\pi}{2})$, no fast acoustic wave can be generated. Second, the existent condition of (9) is deduced.

If $\theta_1 \in (-\frac{\pi}{2}, \frac{\pi}{2})$, $k_{1x} = |k_1|\cos\theta_1 > 0$. Assume that the slow acoustic wave can be generated behind the shock, by using (9), we have

$$\overline{u}_1 k_{1x} = \overline{u}_2 k_{2x} - c_2|k_2| > 0.$$

Then,

$$\frac{k_{2x}}{|k_2|} > \frac{c_2}{\overline{u}_2} = \frac{1}{Ma_{2\mathrm{n}}} > 1. \tag{A1}$$

Since $\cos\theta_2 = \frac{k_{2x}}{|k_2|} \leqslant 1$, there is no solution to (A1), which means that when $\theta_1 \in (-\frac{\pi}{2}, \frac{\pi}{2})$, no slow acoustic wave can be generated.

Similarly, if $\theta_1 \in (\frac{\pi}{2}, \frac{3\pi}{2})$, $k_{1x} = |k_1|\cos\theta_1 < 0$. Assume that the fast acoustic wave can be generated behind the shock. By using (9), we have

$$\overline{u}_1 k_{1x} = \overline{u}_2 k_{2x} + c_2|k_2| < 0.$$

Then, we have

$$\cos\theta_2 = \frac{k_{2x}}{|k_2|} < -\frac{c_2}{\overline{u}_2} = -\frac{1}{Ma_{2\mathrm{n}}} < -1. \tag{A2}$$

Again, (A2) has no solution, which means that when $\theta_1 \in (\frac{\pi}{2}, \frac{3\pi}{2})$, no fast acoustic can be generated behind the shock.

Consider two situations, i.e., $k_y = 0$ and $k_y \neq 0$. If $k_y = 0$, i.e., the incident wave vector is perpendicular to the shock. θ_1 can be 0 or π. When $\theta_1 = 0$, the plus sign is taken in (9), which means that the fast acoustic wave is generated behind the shock, and its wave angle and wave vector are

$$\theta_2 = 0, \quad k_2 = k_{2x} = \frac{\overline{u}_1}{\overline{u}_2 + c_2} k_{1x}.$$

Similarly, when $\theta_1 = \pi$, the minus sign is taken in (9). A slow acoustic wave is generated. Then,

$$\theta_2 = \pi, \quad k_2 = k_{2x} = \frac{\overline{u}_1}{\overline{u}_2 - c_2} k_{1x}.$$

If $k_y \neq 0$, since $|k_2| > 0$, dividing $|k_2|$ on both sides of (9), and making use of

$$\frac{k_{2x}}{|k_2|} = \cos\theta_2, \quad \frac{k_{1x}}{|k_2|} = \frac{k_{1x}}{k_y}\frac{k_y}{|k_2|} = \frac{\sin\theta_2}{\tan\theta_1},$$

(9) can be written as follows:

$$\overline{u}_1 \frac{\sin\theta_2}{\tan\theta_1} = \overline{u}_1\cos\theta_2 \pm c_2. \tag{A3}$$

Square both sides of (A3) and rearrange the terms. Then, we have a quadratic equation of $\cos\theta_2$,

$$\Big(\overline{u}_2^2 + \frac{\overline{u}_1^2}{\tan^2\theta_1}\Big)\cos^2\theta_2 \pm 2\overline{u}_2 c_2\cos\theta_2 + c_2^2 - \frac{\overline{u}_1^2}{\tan^2\theta_1} = 0. \tag{A4}$$

From the existent condition of (A4), i.e., the discriminant is positive, we have

$$\Delta = 4\overline{u}_2^2 c_2^2 - 4\Big(\overline{u}_2^2 + \frac{\overline{u}_1^2}{\tan^2\theta_2}\Big)\Big(c_2^2 - \frac{\overline{u}_1^2}{\tan^2\theta_1}\Big) \geqslant 0.$$

By simplifying the above equation, we can get

$$\tan^2\theta_1 \leqslant \frac{Ma_{1\mathrm{n}}^2}{R^2(1 - Ma_{2\mathrm{n}}^2)},$$

where $R = c_2/c_1$.

There are four solutions of θ_2 to (A4) no matter the plus or minus sign is taken. However, only one is physical, which can be found out by checking the conditions as listed in Subsection 2.2.